IET Renewable Power Generation

Research Article

IET Journals
The Institution of Engineering and Technology

Multiple-input–multiple-output high-order sliding mode control for a permanent magnet synchronous generator wind-based system with grid support capabilities

ISSN 1752-1416
Received on 5th December 2014
Revised on 6th April 2015
Accepted on 9th April 2015
doi: 10.1049/iet-rpg.2014.0417
www.ietdl.org

Fernando Valenciaga[1] ✉, *Roberto Daniel Fernandez*[2]

[1]*Group of Control Applications (GCA), Facultad de Ingeniería, Universidad Nacional de La Plata-CONICET, c.c. 91 C.P, 1900 La Plata, Argentina*
[2]*Facultad de Ingeniería, Universidad Nacional de la Patagonia – SJB, Ruta N1 Km 4, C.P. 9000 Comodoro Rivadavia, Argentina*
✉ *E-mail: fval@ing.unlp.edu.ar*

Abstract: This study presents a control design for a grid connected wind energy conversion system based on a gearless PMSG. The generation system structure comprises a three blade turbine, a 2 MW multi-pole PMSG and a full-scale back-to-back frequency converter linked to the utility grid. The proposed control scheme allows following dynamical specifications taking into account operational requirements and ancillary services imposed by the recent grid connection codes, that is, reactive power regulation and fault ride-through (FRT) capabilities. The control actions to be applied during normal grid operation are designed through second-order sliding mode techniques using a two-stage cascade structure. The multi-variable controller designed attains to regulate the active and reactive powers delivered to the grid, minimising the resistive losses into the generator and maintaining important internal variables into the desired range. This controller presents attractive advantages such as robustness against unmodelled dynamics and external perturbations, finite time convergence to the sliding surfaces and chattering mitigation. To endorse the controlled system with FRT capabilities, a switching control scheme based on voltage grid measurements is also proposed. The performance of the whole control approach is analysed through representative simulations which include parameter variations, external perturbations and three-phase voltage dips.

1 Introduction

During the past two decades the wind energy penetration level has been continuously increasing. This situation has promoted a new generation of grid connection codes with specific technical requirements for the connection of wind energy conversion systems (WECSs) [1, 2]. These relatively recent codes require that wind power stations present similar operational characteristics to those of conventional power plants [3], that is, contribute to power system control (frequency and voltage) taking care of their behaviour in case of abnormal operating conditions of the network (voltage dips). Specifically, the most common requirements include fault ride-through (FRT) capability, extended system voltage and frequency variation limits, active power regulation and frequency control, as well as reactive power/power factor and voltage regulation capabilities [2–6]. The final objective of these demands is to guarantee a safe and reliable grid operation, stabilising the wind turbine behaviour and decreasing the amount of wind power to be lost following system disturbances [2].

Variable speed WECSs based on multipolar permanent magnet synchronous generators (PMSGs) are emerging as a robust alternative to grid connected wind systems based on the doubly fed induction generator [7–10]. Topologically, these systems are usually linked to the utility grid through a full-rated back-to-back converter with an intermediate direct current bus (DC-bus) to facilitate the necessary frequency conversion between the generator and the grid (see Fig. 1). The main advantages of this configuration are: its wide speed range of operation, direct control of active and reactive powers delivered to the grid, reduced mechanical stress, higher efficiency, robustness and better power factor than its counterparts and full control over the generator and the grid side converter for network support during faults [4, 7, 11].

In the outlined regulation context, successful control strategies directed to fulfil local grid codes requirements are essential. Regulation of the active and reactive powers injected by WECS into the grid and mitigation of internal instability during abnormal grid operation directed to help for a fast grid fault recovery, become critical control targets. In this sense, structures linked to the grid via full-rated converters produce a natural and relative decoupling between the grid and the generator which is not directly subject to grid faults [7, 12]. Besides, it has been proved that switching some of the traditional control objectives between both static converters produces a better FRT recovery [12, 13]. Following these general guidelines, the proposed control permits to regulate the DC-bus voltage and the active and reactive powers injected into the grid (maximising the wind power conversion) and also to minimise the resistive generator losses [14]. In case of grid faults (three-phase voltage dips), automatic control changes avoid internal instabilities and large currents on the grid side inverter.

Second-order sliding mode (SOSM) techniques and specifically the super-twisting algorithm (STwA) approach [15, 16] are used to synthesize a fixed gains multiple-input–multiple-output (MIMO) controller that fulfil the desired control objectives. This theoretical framework presents a set of attractive advantages that cover most of the requirements necessary for this case. Briefly, the resultant controllers have a high robustness degree to unmodelled dynamics and continuous bounded perturbations, present a bounded and finite reaching time, have a very simple structure with a low computational burden, are very appropriate to successfully deal with the control design for non-linear complex systems and, ideally, they do not present ripple (chattering) on the sliding surfaces [17–19].

The main contribution of this paper is to present a simple and robust control scheme that allows fulfilling not only dynamic control objectives but also provides ancillary services to the utility

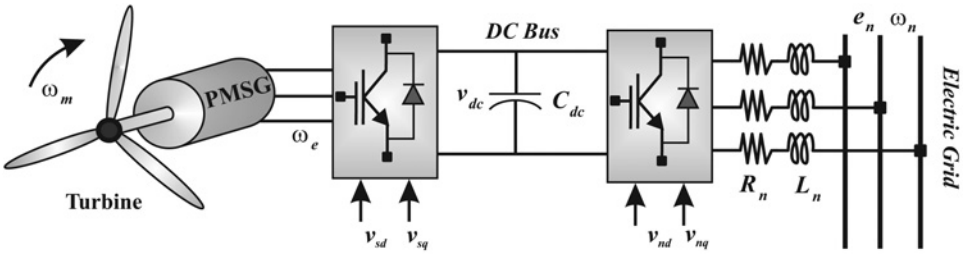

Fig. 1 *Structure of the PMSG–WECS*

grid. The proposed scheme is based on a two-layers MIMO–SOSM–STwA controller immersed in a switching context structure that allows effectively dealing with multiple and simultaneous control objectives and also with some common grid faults such as three-phase voltage dips. The designed controller takes into account the complex non-linear system dynamics as well as uncertainties in the model and bounded but unknown external perturbations. The resultant control action is very simple to implement with a low computational cost and contrary to linear control approaches, presents a continuous performance in the whole operational range considered during the design stage.

This paper is organised as follows: in Section 2 the structure of the PMSG–WECS is analysed producing a seventh-order non-linear dynamic system model. Section 3 is devoted to present the control objectives, their assignment and implementation. After this, general guidelines for the design of MIMO–SOSM–STwA are presented and finally in Section 4, the performance of the control proposal is analysed through representative simulations including normal and abnormal grid operations.

2 System dynamic modelling

The core of the WECS depicted in Fig. 1 is composed of a wind turbine directly linked to a multipolar PMSG connected to the grid through a full-rated back-to-back converter. The multipolar magnetic rotor of this generator allows a simpler mechanical assembling because slip rings and gearbox are not necessary. This distinctive feature reduces maintenance costs and endows the structure with better robustness features. On the other hand, the back-to-back static converter permits to adapt voltages and frequencies between the generator terminals and the grid without reactive power exchange between them.

The electric dynamics equations corresponding to a PMSG with non-salient poles, small air-gap and a sinusoidal magnetic flux spatial profile can be written in a rotating reference frame aligned with the magnetic axis of the rotor as

$$\dot{i}_{sd} = \frac{1}{L_{sd}}\left(-R_s i_{sd} + \omega_e L_{sq} i_{sq} - v_{sd}\right) \tag{1}$$

$$\dot{i}_{sq} = \frac{1}{L_{sq}}\left(-R_s i_{sq} - \omega_e L_{sd} i_{sd} + \omega_e \Phi_{PM} - v_{sq}\right) \tag{2}$$

where i_{sd}–i_{sq} are the direct and quadrature currents components in the stator windings, ω_e is the electrical angular frequency and v_{sd}–v_{sq} are the voltage components on the generator terminals. The parameters R_s, L_{sd} and L_{sq} are the stator winding resistance and the direct and quadrature inductances and Φ_{PM} is the magnetic flux acting on the stator windings. The active and reactive powers delivered by this generator can be, respectively, expressed by

$$P_g = \frac{3}{2}(v_{sd} i_{sd} + v_{sq} i_{sq}) \tag{3}$$

$$Q_g = \frac{3}{2}(v_{sq} i_{sd} - v_{sd} i_{sq}) \tag{4}$$

The mechanical shaft dynamics is modelled through a two-mass scheme characterised by stiffness and damping coefficients k and c, respectively. This flexible shaft is considered stiff on the turbine side because of its high inertia (J_t), acting then as a torsion spring on the generator side which presents a lower inertia value (J_g). The mechanical behaviour of the rotating parts is given by

$$\dot{\omega}_{mt} = \left(T_t(\omega_e,\ v) - T_{tw}(\Delta\omega,\ \Delta\theta)\right)/J_t \tag{5}$$

$$\dot{\omega}_{mg} = \left(T_{tw}(\Delta\omega,\ \Delta\theta) - \frac{3}{2}\frac{P}{2}\Phi_{PM} i_{sq}\right)\Big/ J_g \tag{6}$$

where T_t is the impulsive torque produced by the turbine, ω_{mt} and ω_{mg} are the mechanical angular speeds on the shaft extremes (turbine and generator, respectively) being θ_{mt} and θ_{mg} their respective angular position values and $T_{tw}(\Delta\omega, \Delta\theta) = c(\omega_{mt} - \omega_{mg}) + k(\theta_{mt} - \theta_{mg})$. It should be noted that the generator angular speed is related to its electrical angular speed as $\omega_e = P\omega_{mg}/2$, where P is the total pole number.

The turbine torque T_t in (5) depends on several variables and parameters. It is related to the mechanical power developed by the turbine through

$$P_t(\omega_e,\ v) = T_t \omega_{mt} = \frac{1}{2}\rho A C_p v^3 \tag{7}$$

where ρ is the air density, A is the cross-section area swept by the turbine, v is the wind speed and C_p is a turbine coefficient that takes into account its conversion efficiency. This last coefficient is usually written as a function of the tip speed ratio $\lambda = R\omega_m/v$ and the attitude angle β [20]

$$C_p(\lambda,\ \beta) = c_1\left(\frac{c_2}{\vartheta} - c_3\beta - c_4\right)e^{-(c_5/\vartheta)} \tag{8}$$

where $(1/\vartheta) = (1/(\lambda + 0.08\beta)) - (0.035/1 + \beta^3)$ and c_1, c_2 c_3, c_4 and c_5 are coefficients that characterise each turbine design.

The DC-bus dynamic behaviour can be completely described through the voltage on C_{dc}. Considering mean values, the dynamic voltage expression obtained from the input/output active power balance is

$$\dot{v}_{dc} = \frac{3\left((v_{sd} i_{sd} + v_{sq} i_{sq}) - (v_{nd} i_{nd} + v_{nq} i_{nq})\right)}{2 v_{dc} C_{dc}} \tag{9}$$

where i_{nd} and i_{nq} are the components of the spatial vector of current in a grid synchronous frame rotating with angular speed ω_n and aligned with the grid voltage spatial vector. In this context, the components of the voltage vector on the inverter terminals are, respectively, denoted as: v_{nd} and v_{nq}.

IET Renew. Power Gener., 2015, Vol. 9, Iss. 8, pp. 925–934

Finally, using the previously specified rotating frame the power exchanged with the grid can be described through the equations

$$\dot{i}_{nd} = \left(-R_n i_{nd} + \omega_n L_n i_{nq} + v_{nd} - e_n\right)\Big/ L_n \tag{10}$$

$$\dot{i}_{nq} = \left(-R_n i_{nq} - \omega_n L_n i_{nd} + v_{nq}\right)\Big/ L_n \tag{11}$$

where e_n, R_n and L_n are, respectively, the voltage, resistance and inductance corresponding to the grid equivalent Thevenin circuit. The active and reactive powers delivered to the grid can be written as

$$P_n = \frac{3}{2} e_{nd} i_{nd} \tag{12}$$

$$Q_n = \frac{3}{2} e_{nd} i_{nq} \tag{13}$$

It should be noted that these powers are naturally decoupled because they depend on different quadrature current components.

Summarising, the complete grid connected PMSG–WECS can be described by a ninth-order dynamic model which in the compact non-linear affine form may be written as: $\dot{\boldsymbol{x}} = \boldsymbol{F}(\boldsymbol{x}) + \boldsymbol{G}(\boldsymbol{x})\boldsymbol{u}$ where $\boldsymbol{x} = [i_{sd}\ i_{sq}\ \theta_{\mathrm{mt}}\ \omega_{\mathrm{mt}}\ \theta_{\mathrm{mg}}\ \omega_{\mathrm{mg}}\ v_{\mathrm{dc}}\ i_{nd}\ i_{nq}]^{\mathrm{T}}$ and $\boldsymbol{u} = [v_{sd}\ v_{sq}\ v_{nd}\ v_{nq}]^{\mathrm{T}}$

$$\boldsymbol{F}(\boldsymbol{x}) = \begin{bmatrix} \dfrac{-R_{\mathrm{s}} i_{sd} + \omega_{\mathrm{e}} L_{sq} i_{sq}}{L_{sd}} \\ \dfrac{-R_{\mathrm{s}} i_{sq} - \omega_{\mathrm{e}} L_{sd} i_{sd} + \omega_{\mathrm{e}} \Phi_{\mathrm{PM}}}{L_{sq}} \\ \omega_{\mathrm{mt}} \\ \dfrac{(P/2)\left(T_{\mathrm{t}}(\omega_{\mathrm{e}},\ \nu) - T_{tw}(\Delta\omega,\ \Delta\theta)\right)}{J_{\mathrm{t}}} \\ \omega_{\mathrm{mg}} \\ \dfrac{T_{tw}(\Delta\omega,\ \Delta\theta) - (3/2)(P/2)\Phi_{\mathrm{PM}} i_{sq}}{J_{\mathrm{g}}} \\ 0 \\ \dfrac{-R_n i_{nd} + \omega_n L_n i_{nq} - e_n}{L_n} \\ \dfrac{-R_n i_{nq} - \omega_n L_n i_{nd}}{L_n} \end{bmatrix} \tag{14}$$

and

$$\boldsymbol{G}(\boldsymbol{x}) = \begin{bmatrix} -\dfrac{1}{L_{sd}} & 0 & 0 & 0 \\ 0 & -\dfrac{1}{L_{sq}} & 0 & 0 \\ 0 & 0 & 0 & 0 \\ 0 & 0 & 0 & 0 \\ 0 & 0 & 0 & 0 \\ 0 & 0 & 0 & 0 \\ \dfrac{3 i_{sd}}{2 v_{\mathrm{dc}} C_{\mathrm{dc}}} & \dfrac{3 i_{sq}}{2 v_{\mathrm{dc}} C_{\mathrm{dc}}} & -\dfrac{3 i_{nd}}{2 v_{\mathrm{dc}} C_{\mathrm{dc}}} & -\dfrac{3 i_{nq}}{2 v_{\mathrm{dc}} C_{\mathrm{dc}}} \\ 0 & 0 & \dfrac{1}{L_n} & 0 \\ 0 & 0 & 0 & \dfrac{1}{L_n} \end{bmatrix} \tag{15}$$

These last matrixes explicitly show the non-linear complex nature of the system model.

3 Control design

Nowadays, besides the generation requisites WECS are required to overcome some kind of grid failures without disconnection and, at the same time, to provide ancillary services during normal operation in order to help for the grid stability (frequency and voltage maintenances). PMSG–WECS structures such as the presented in Fig. 1 are usually operated employing a typical control assignment, that is, using the grid inverter to regulate the reactive power delivered to the net and the DC-bus voltage, whereas the generator side converter is used to regulate the active power generation. However, recent studies have determined that the interchange of some of the control roles between the static converters results beneficial to the system stability, especially in the presence of some kind of grid failures [12, 13]. Following this current tendency, the proposed control strategy employs the following control assignment: the grid side inverter regulates the active and reactive powers delivered to the grid while the generator side inverter is responsible for keeping the DC-bus voltage and minimising the resistive losses into the PMSG.

In the next sections, the development of a multi-variable controller capable to fulfil the mentioned desired objectives is presented. This controller is designed from the SOSM theoretical framework which is very appropriate to deal with systems described by uncertain non-linear dynamic models subjected to external perturbations. In particular, this technique generates robust and simple controllers with reduced chattering effects on the sliding surfaces and, in the specific case of STwA realisations, synthesising continuous control actions [17, 18, 21]. The resultant controllers do not depend on the system parameter values and naturally assimilate their bounded temporal drifts.

To proceed with the controller design, the desired control objectives must be expressed in terms of analytical sliding variables. The main restriction in this procedure is to obtain a set of sliding surfaces that fulfil the necessary vectorial relative degree (VRD) condition, that is, VRD = [1 1 1 … 1]. Considering this and taking into account (12) and (13), the control objectives for the grid side inverter can be expressed as

$$s_1 = P_{\mathrm{ref}} - \frac{3}{2} e_{nd} i_{nd} \tag{16}$$

$$s_2 = Q_{\mathrm{ref}} - \frac{3}{2} e_{nd} i_{nq} \tag{17}$$

where the active power reference P_{ref} can be a constant value externally fixed (in case of following a power regulation scheme) or a variable reference to follow the maximum energy conversion point [22]. Taking this last option

$$P_{\mathrm{ref}} = \eta_1 \frac{4\rho A \hat{C}_p R^3 \omega_{\mathrm{e}}^3}{P^3 \lambda_{\mathrm{opt}}^3} \tag{18}$$

It should be observed that this reference is a filtered version of the real maximum power profile, scaled by a constant $\eta_1 < 1$ to take into account mechanical and electrical power leakages. With respect to the sliding variable s_2, it considers a reactive power reference determined by the grid operator according to stability issues.

The generator side inverter is in charge of keeping the DC-bus voltage and minimising the resistive losses. This last control objective is equivalent to cancel the reactive power on the generator terminals which implies to impose an algebraic relationship between the control variables v_{sd} and v_{sq} given by (see (4))

$$v_{sd} = v_{sq} \frac{i_{sd}}{i_{sq}} \tag{19}$$

reducing in one degree the order of the control vector.

To control the DC-bus voltage the nested SOSM–STwA controller scheme shown in Fig. 2 is proposed. This structure simultaneously works on two sliding variables that can be

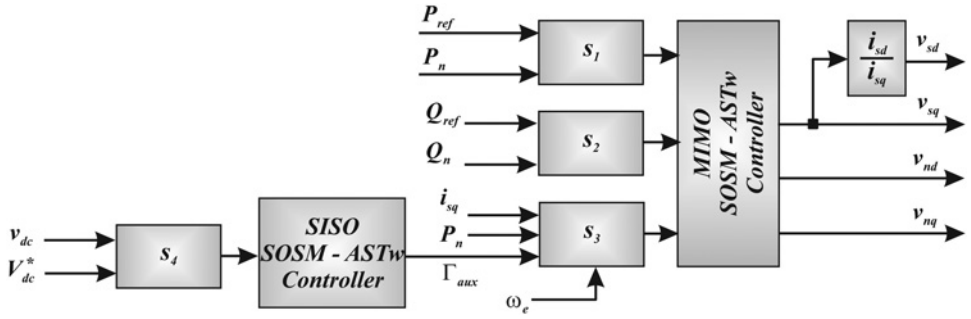

Fig. 2 *Control scheme*

expressed as

$$s_3 = I^*_{sq} - i_{sq} = \underbrace{\frac{2P_n}{3\Phi_{\rm PM}\omega_{\rm e}} + \Gamma_{\rm aux}}_{I^*_{sq}} - i_{sq} \tag{20}$$

$$s_4 = v_{\rm dc} - V^*_{\rm dc} \tag{21}$$

where $\Gamma_{\rm aux}$ is the output of the controller operating on s_4. The proposed scheme uses in (20) a reference (I^*_{sq}) composed by two terms. The first one corresponds to the necessary current i_{sq} to balance the mechanical power generated by the PMSG and the active power delivered to the grid. Obviously, this reference is omitting different electromechanical losses and initial DC-bus voltage error. Therefore it is necessary to include an auxiliary reference term ($\Gamma_{\rm aux}$) to compensate model distortions and inaccuracies. In particular, $\Gamma_{\rm aux}$ allows adjusting the reference I^*_{sq} using the errors on s_4 but in a filtered way because of the action of the controller acting on this last surface (first layer of the nested scheme). Thus, the system convergence on s_1, s_2 and s_3 is much faster than the convergence on s_4 which also involves the relatively slow temporal behaviour of $C_{\rm dc}$.

It is important to remark that s_4 fulfils all the requirements to be directly used by an SOSM controller to regulate the DC-bus voltage. However, when the system tries to follow relative fast active power excursions, such a control structure produces an unacceptable ripple on this sliding variable. The proposed control scheme avoids this behaviour presenting a very good dynamic performance.

3.1 MIMO–SOSM controller design

Taking into account the different temporal scales into the dynamic system and the nested control structure, the controller design can be tackled in two steps. The first one involves the design of a MIMO SOSM controller acting on s_1, s_2 and s_3. In this stage, it is considered that $\Gamma_{\rm aux}$ in (20) remains constant. In the second step, the single-input–single-output (SISO) SOSM control design on s_4 is addressed considering that the system is already working on the intersection of the first three surfaces. The very slow dynamics of s_4 completely justify this assumption.

To proceed with the MIMO–SOSM design, the non-linear affine dynamics system model determined by the matrixes (14) and (15) is firstly reduced by the use of the algebraic control relationship (19) and written in the following compact form

$$\dot{\boldsymbol{x}} = \underbrace{\boldsymbol{F}(\boldsymbol{x}) + \Delta\boldsymbol{F}(\boldsymbol{x},\ t) + \boldsymbol{\xi}(t)}_{\widetilde{\boldsymbol{F}}} + \boldsymbol{G}\boldsymbol{u} \tag{22}$$

where $\boldsymbol{x} \in \Re^n$ is the states vector and $\boldsymbol{u} \in \Re^m$ is the control vector, $\boldsymbol{F}$ represents the nominal drift vector, $\Delta\boldsymbol{F}(\boldsymbol{x}, t)$ is produced by unknown slow temporal parameter variations acting on the drift vector, $\boldsymbol{\xi}(t)$ represents the influence of bounded and continuous external perturbations and finally $\boldsymbol{G} = [\boldsymbol{g}_1\ \boldsymbol{g}_2\ \boldsymbol{g}_3]$ is the system control matrix. Then, considering the sliding vector $\boldsymbol{S} = [s_1,\ s_2,\ s_3]^{\rm T}$ it is straightforward to obtain $\dot{\boldsymbol{S}}$ as

$$\dot{\boldsymbol{S}} = \begin{bmatrix} L_{\tilde{F}}s_1 \\ L_{\tilde{F}}s_2 \\ L_{\tilde{F}}s_3 \end{bmatrix} + \begin{bmatrix} 0 & L_{g_2}s_1 & 0 \\ 0 & 0 & L_{g_3}s_2 \\ L_{g_1}s_3 & L_{g_2}s_3 & 0 \end{bmatrix} \begin{bmatrix} v_{sq} \\ v_{nd} \\ v_{nq} \end{bmatrix} \tag{23}$$

where the Lie derivatives of the first vector corresponds to continuous bounded functions. On the other hand

$$\begin{aligned} L_{g_2}s_1 &= -\frac{3e_{nd}}{2L_n} \qquad L_{g_3}s_2 = -\frac{3e_{nd}}{2L_n} \\ L_{g_1}s_3 &= \frac{1}{L_{qn}} \qquad L_{g_2}s_3 = \frac{e_{nd}}{L_n\Phi_{\rm PM}\omega_{\rm e}} \end{aligned} \tag{24}$$

It is important to note that the proposed sliding vector determines in (23) a control matrix that simplifies the control design task because there is a unique possible control assignment, implicitly imposed by the system structure [16]. In this sense v_{nq}, v_{sq} and v_{nd} are the only control actions to drive the system towards $s_1 = 0$, $s_2 = 0$ and $s_3 = 0$, respectively.

From (23), the second time derivative of $\boldsymbol{S}$ can be written as

$$\begin{aligned} \ddot{\boldsymbol{S}} = &\begin{bmatrix} L^2_{\tilde{F}}s_1 + \dfrac{\partial L_{\tilde{F}}s_1}{\partial t} \\ L^2_{\tilde{F}}s_2 + \dfrac{\partial L_{\tilde{F}}s_2}{\partial t} \\ L^2_{\tilde{F}}s_3 + \dfrac{\partial L_{\tilde{F}}s_3}{\partial t} \end{bmatrix} + \begin{bmatrix} L_{g_1}L_{\tilde{F}}s_1 & L_{g_2}L_{\tilde{F}}s_1 & L_{g_3}L_{\tilde{F}}s_1 \\ L_{g_1}L_{\tilde{F}}s_2 & L_{g_2}L_{\tilde{F}}s_2 & L_{g_3}L_{\tilde{F}}s_2 \\ L_{g_1}L_{\tilde{F}}s_3 & L_{g_2}L_{\tilde{F}}s_3 & L_{g_3}L_{\tilde{F}}s_3 \end{bmatrix} \\ &\times \begin{bmatrix} v_{sq} \\ v_{nd} \\ v_{nq} \end{bmatrix} + \begin{bmatrix} 0 & L_{g_2}s_1 & 0 \\ 0 & 0 & L_{g_3}s_2 \\ L_{g_1}s_3 & L_{g_2}s_3 & 0 \end{bmatrix} \begin{bmatrix} \dot{v}_{sq} \\ \dot{v}_{nd} \\ \dot{v}_{nq} \end{bmatrix} \end{aligned} \tag{25}$$

Given that all the expressions involved in (25) correspond to continuous bounded functions, considering the operational limits of the system and the general features of the acting disturbances, there can be found three sets of constants $\underline{K}_{s_i}$, $\bar{K}_{s_i}$, C_{s_i}, U_{M_i} and q_{s_i} with $i = 1,\ 2,\ 3$ and, respectively, $j = 2,\ 3,\ 1$ (pairs i–j determine the control assignments) that fulfil the inequalities

$$0 < q_{s_i} < 1 \tag{26}$$

$$0 < \underline{K}_{s_i} < L_{g_j}s_i < \bar{K}_{s_i} \tag{27}$$

$$\begin{aligned} &\left|L^2_{\tilde{F}}s_i + \frac{\partial L_{\tilde{F}}s_i}{\partial t}\right| + \sum_{k=1}^{3}\left|L_{g_k}L_{\tilde{F}}s_i\right|U_{M_k} \\ &\quad + \sum_{k\neq j}\left|L_{g_k}s_i\right|\bar{u}_k \le C_{s_i} \end{aligned} \tag{28}$$

IET Renew. Power Gener., 2015, Vol. 9, Iss. 8, pp. 925–934

$$\left|\frac{L_{\tilde{F}}s_i + (\partial s_i/\partial t) + \sum_{k\neq j} L_{g_k}s_i U_{M_k}}{L_{g_j}s_i}\right| < q_{s_i}U_{M_i} \tag{29}$$

Taking into account (26)–(29), it is straightforward to see that each second time derivative $\ddot{s}_i$ of (25) belongs to the differential inclusion

$$\ddot{s}_i \in \left[-C_{s_i},\ C_{s_i}\right] + \left[\underline{K}_{s_i},\ \bar{K}_{s_i}\right]\nu_i \tag{30}$$

where ν_i is the corresponding control time derivative. This differential inclusion contains the nominal system dynamics and all its possible deviations produced by the set of considered bounded perturbations and parameter variations acting on the system in its whole operational range. The limits of this differential inclusion will correspond to the worst combinations of unmodelled dynamics and external perturbations. Then, if the parameters α_{s_i} and γ_{s_i} are chosen according to the inequalities

$$\underline{K}_{s_i}\alpha_{s_i} > C_{s_i} \tag{31}$$

$$\gamma_{s_i} > \sqrt{\frac{2}{\underline{K}_{s_i}\alpha_{s_i} - C_{s_i}}}\,\frac{\bar{K}_{s_i}(\underline{K}_{s_i}\alpha_{s_i} - C_{s_i})(1-q_{s_i})}{\underline{K}_{s_i}^2(1+q_{s_i})} \tag{32}$$

the SOSM–STwA controller

$$u_i = -\gamma_{s_i}|s_i|^{1/2}\,\mathrm{sign}(s_i) + \nu_i \tag{33}$$

$$\dot{\nu}_i = \begin{cases} -u_i, & |u_i| > U_{M_i} \\ -\alpha_{s_i}\,\mathrm{sign}(s_i), & |u_i| \le U_{M_i} \end{cases} \tag{34}$$

provides for the finite time system convergence of any system in (30) to the manifold $s_i = \dot{s}_i = 0 \quad i = 1,\ 2,\ 3$, being the reaching time a locally bounded function of the initial conditions [23]. This means that the resultant controllers are robust against the set of perturbations and parameter variations considered because they cannot take the system dynamics outside of this differential inclusion. The perturbed system evolution will always be contained in (30) ensuring the finite time convergence. Once the system is in sliding mode, the motion is characterised by chattering absence.

In this particular case, the controller parameters α_i, γ_i and U_{Mi}, and consequently bounds (26)–(29), can be determined in any arbitrary order of $i = 1,\ 2,\ 3$, because of the triangular control matrix nature [24]. The design process starts doing a detailed analysis of the expressions involved in (25) which must take into account the unmodelled dynamics ($\Delta\boldsymbol{F}(\boldsymbol{x},\ t)$) and perturbations terms ($\boldsymbol{\xi}(t)$). The objective of this first analysis is to find (after a long but straightforward algebraic process) some conservative bounds corresponding to the constants that determine the differential inclusion limits (C_{s_i}, $\underline{K}_{s_i}$ and $\bar{K}_{s_i}$). This process is carried out regarding the operational limits and the maximum levels of perturbations and unmodelled dynamics acting on the system, looking for the worst cases. Then, the parameters of the controller for each sliding surface can be selected according to expressions (31) and (32) to obtain a good reaching performance. This last tuning phase is commonly realised only once during the process design, complementing analytic and simulation tools [25]. The on-line computational burden of this kind of controllers is in fact very low (see (33)), comparable with PID implementations but presenting outstanding robustness features.

3.2 SISO–SOSM controller design

The second step on the design process is to synthesize an SISO–SOSM controller that allows to fulfil the condition $s_4 = \dot{s}_4 = 0$ in finite time considering that the system is already operating on the manifold $s_1 = s_2 = s_3 = 0$. This last condition imposes some algebraic restrictions among the system states, determining a reduction in the model order. Thus, the new dynamic system representation assumes an SISO six-degree of freedom non-affine structure under the general form $\dot{x} = f(x,\ u)$ with $x = [i_{sd}\ \theta_{\mathrm{mt}}\ \omega_{\mathrm{mt}}\ \theta_{\mathrm{mg}}\ \omega_{\mathrm{mg}}\ v_{\mathrm{dc}}]^{\mathrm{T}}$ and $u = \Gamma_{\mathrm{aux}}$.

The new system form determines that $\dot{s}_4$ does not present the necessary structure to be tackled through SOSM techniques. To overcome this problem, the system must be expressed in a control affine form. Using the Taylor's development around the nominal operating point, the following approximation can be used

$$\dot{\boldsymbol{x}} \simeq \underbrace{\boldsymbol{F}(\boldsymbol{x}_{\mathrm{op}},\ u_{\mathrm{op}}) + \Upsilon(\boldsymbol{x},\ \boldsymbol{x}_{\mathrm{op}},\ u_{\mathrm{op}})}_{\eta(\boldsymbol{x})} + \underbrace{\frac{\partial \boldsymbol{F}(\boldsymbol{x}_{\mathrm{op}},\ u_{\mathrm{op}})}{\partial u}}_{\varrho}\underbrace{(u - u_{\mathrm{op}})}_{\tilde{u}} \tag{35}$$

where function Υ is considering all the Taylor's terms on $\boldsymbol{x}$. Then, the first temporal derivative of s_4 can be approximated as

$$\dot{s}_4 = \frac{\partial s_4}{\partial \boldsymbol{x}}\,\eta(\boldsymbol{x}) + \frac{\partial s_4}{\partial \boldsymbol{x}}\,\varrho\tilde{u} \tag{36}$$

Given that s_4 only depends on the variable v_{dc}, only the terms in the last line of (35) are involved in (36), reducing the complexity of this expression. Then, following the same steps that for the MIMO case, there can be found a set of constants $\underline{K}_{s_4}$, $\bar{K}_{s_4}$, C_{s_4}, U_{M_4} and q_{s_4} that fulfil the inequalities

$$0 < q_{s_4} < 1 \tag{37}$$

$$0 < \underline{K}_{s_4} < \frac{\partial s_4}{\partial \boldsymbol{x}}\,\varrho < \bar{K}_{s_4} \tag{38}$$

$$\left|\left(\frac{\partial s_4}{\partial \boldsymbol{x}}\,\eta(\boldsymbol{x})\right)\right| + \left|\left(\frac{\partial s_4}{\partial \boldsymbol{x}}\,\varrho\right)\right| U_{M_4} \le C_{s_4} \tag{39}$$

$$\left|\left(\frac{\partial s_4}{\partial \boldsymbol{x}}\,\eta(\boldsymbol{x})\right) \Big/ \left(\frac{\partial s_4}{\partial \boldsymbol{x}}\,\varrho\right)\right| < q_{s_4}U_{M_4} \tag{40}$$

for the considered operational range around the nominal point. Therefore according to the SOSM–STwA, if the parameters α_{s_4} and γ_{s_4} are chosen keeping the inequalities

$$\underline{K}_{s_4}\alpha_{s_4} > C_{s_4} \tag{41}$$

$$\gamma_{s_4} > \sqrt{\frac{2}{\underline{K}_{s_4}\alpha_{s_4} - C_{s_4}}}\,\frac{\bar{K}_{s_4}(\underline{K}_{s_4}\alpha_{s_4} - C_{s_4})(1-q_{s_4})}{\underline{K}_{s_4}^2(1+q_{s_4})} \tag{42}$$

the SOSM–STwA controller

$$u_4 = -\gamma_{s_4}|s_4|^{1/2}\,\mathrm{sign}(s_4) + \nu_4 \tag{43}$$

$$\dot{\nu}_4 = \begin{cases} -u_4, & |u_4| > U_{M_4} \\ -\alpha_{s_4}\,\mathrm{sign}(s_4), & |u_4| \le U_{M_4} \end{cases} \tag{44}$$

provides for the finite time system convergence of the perturbed system to the manifold $s_4 = \dot{s}_4 = 0$, being the reaching time a locally bounded function of the initial conditions [23]. This design procedure determines that the resultant controller is robust against the set of perturbations and parameter variations preserving the differential inclusion implicit in the bounds (37)–(40). Finally, it should be emphasised that the sign function in (43) must be replaced by a trigonometric approximation (tangent function) to avoid discontinuities on the reference I_{sq}^{*} of s_3. Such as in the MIMO case, the parameters of the controller are determined complementing analytic and simulation tools.

3.3 FRT design

As it was previously emphasised, according to the main operation grid codes large WECS must be capable to overcome some typical network disturbances and also provide extra ancillary services to

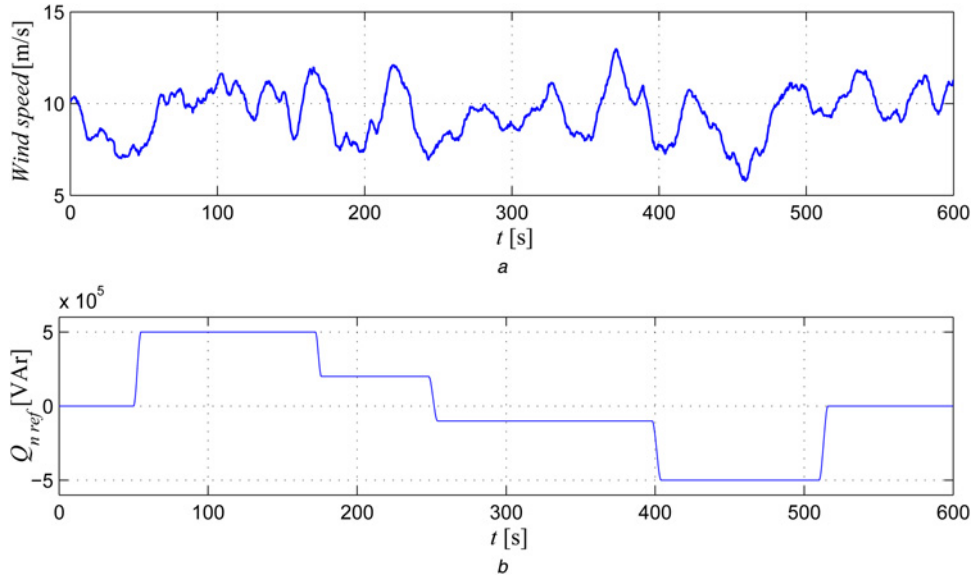

Fig. 3 *External variables*

a Wind speed profile (v)
b Reactive power demand ($Q_{n_{ref}}$)

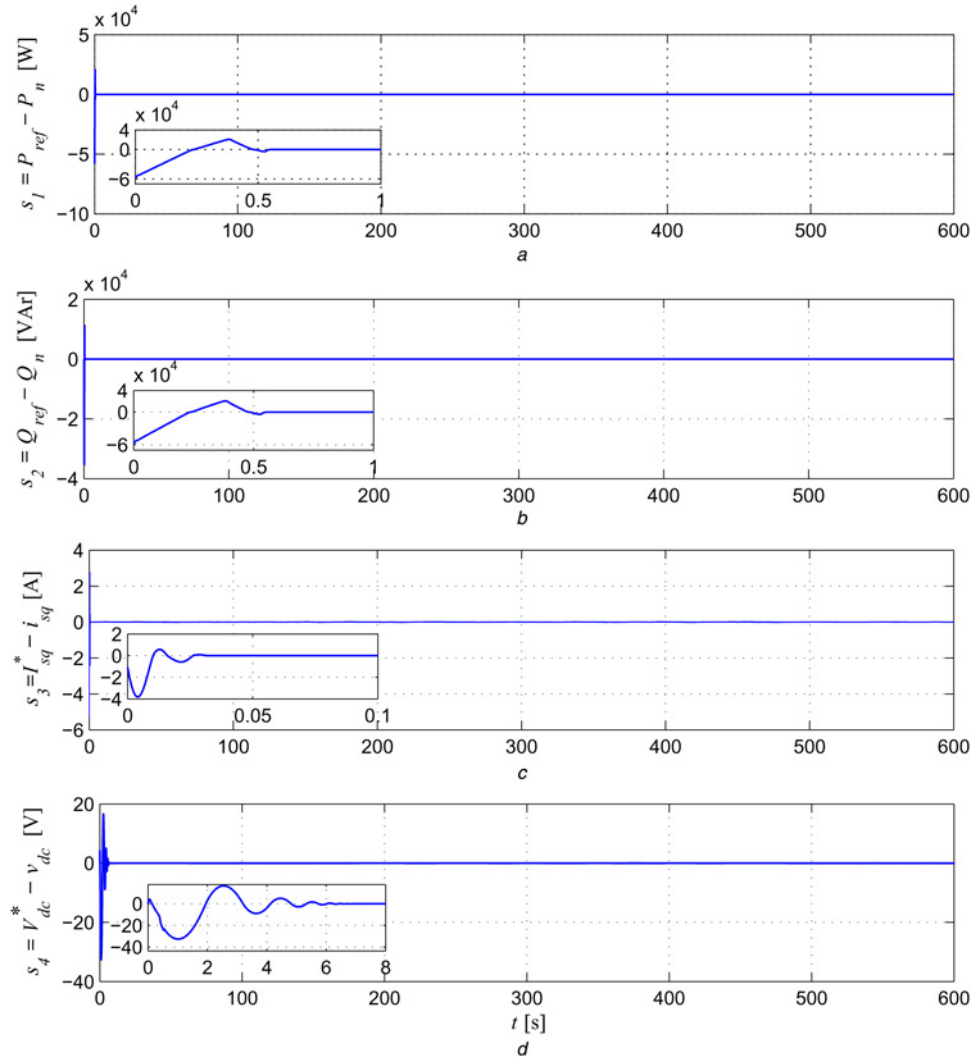

Fig. 4 *Sliding variables profiles*

a s_1
b s_2
c s_3
d s_4

IET Renew. Power Gener., 2015, Vol. 9, Iss. 8, pp. 925–934

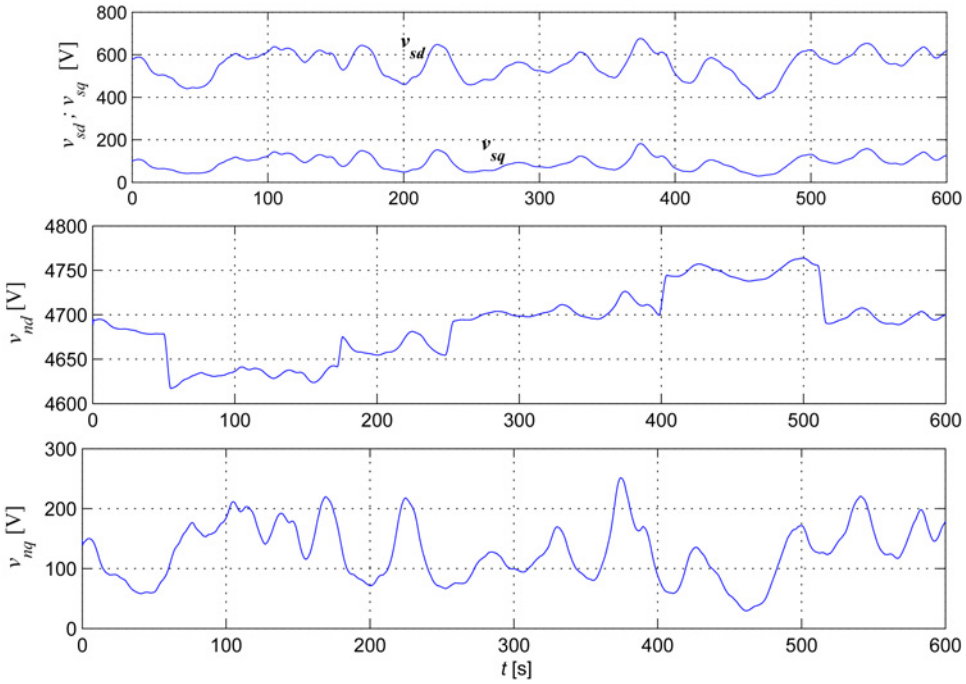

Fig. 5 *Control variables v_{sd}, v_{sq}, v_{nd} and v_{nq}*

help for the network stability [1, 2, 12]. Despite the treatment of all the possible grid faults is beyond the scope of this paper, it is interesting to present some possible control strategies to deal with three-phase grid faults (3PGF) which have the biggest impact on the wind turbine system [1, 17]. In this sense, the pursued objective is to stimulate a new generation of WECS with FRT capabilities capable to avoid disconnections and their associated energy losses.

In this context, the control scheme previously developed is slightly modified in this section to successfully provide the system with FRT capabilities. It is important to note that the main consequence that three-phase voltage dips produce on this kind of WECS is a sudden unbalance between the generated and the delivered active powers. This unbalance is responsible for producing overvoltages on the DC-bus and over speeds on the wind turbine shaft which can finally conduce to destabilise the system, forcing the operator to shut it down.

The proposed switched scheme is based on grid voltage measurements [3–5]. In particular when a 3PGF causes a drop of the voltage component v_{d} below a tolerable value (90% of its rated value) it triggers a set of control structure changes that helps to avoid potential disruptive consequences (over-voltages on the DC-bus, over-currents on the grid inverter and over speeds on the turbine shaft). In this sense, during 3PGF the following actions are taken:

- The SOSM–STwA controllers acting on the grid inverter are replaced by feed-forward controllers obtained from (10) and (11). These new controllers try to maintain the same currents levels that the ones before the fault.
- The inputs of the SOSM–STwA controllers acting on the grid side inverter are forced to zero during the 3PGF to avoid wind-up effects on the controllers outputs. In this way, after a grid fault, the outputs of the controllers will be near to the correct values.

4 Simulation results

Representative computer simulations were conducted to evaluate the performance of the proposed control scheme on a system composed by a 2 MW PMSG taken from [26]. To recreate real simulation conditions the selected examples involve a variable wind speed profile, a variable reactive power grid requirement (see Fig. 3), the presence of unmodelled dynamic through slow variable parameters (electric PMSG (R_{s}, L_{sd} and L_{sq}) and grid parameters (R_n and L_n) were continuously changed within a range of 20% of their rated values) and the influence of continuous bounded external perturbations.

The behaviour of the controller is then examined through two examples. The first one analyses the system behaviour during normal operation and the second during a normalised 3PGF.

4.1 Normal operation

The closed-loop system behaviour can be analysed through the sliding variables whose temporal profiles are presented in Fig. 4. It can be appreciated that the designed controllers are capable to maintain the system on the intersection of all the surfaces without significant chattering even when the simulations are carried out using fixed step algorithms. On the other hand, this last figure shows the different convergence speeds among the controllers as it was specified in the design section. The MIMO–SOSM controller (s_1, s_2 and s_3) presents a fast convergence speed while the SISO–SOSM controller, acting on the DC-bus voltage, drives the system towards $s_4 = 0$ with a slower dynamics. All the excursions around the surfaces during the convergence period present the typical profiles produced by SOSM–STwA-based controllers.

To complete the analysis, Figs. 5 and 6 depict the temporal profiles of the control variables and the system states, respectively. In Fig. 5, it can be appreciated the smoothness of the control variables. This last feature is specially attractive because of implementation issues. On the other hand, it is important to highlight the very good regulation achieved on the DC-bus voltage (see Fig. 6).

Finally, Fig. 7 shows the temporal profiles corresponding to the available wind power on the shaft (blue solid line), the active power injected in the DC-bus (red dashed line) and the active power transmitted to the grid (green dashed line). It can be appreciated that these last two profiles are almost coincident and that they are smooth and delayed with respect to the mechanical power. These last features arise because the control system uses an indirect active power reference obtained from the shaft speed [22].

4.2 Operation during 3PGF

This simulation example examines the system behaviour during a 3PGF produced at $t = 1$ s and characterised by a 90% voltage drop of 250 ms. According with the control strategy presented in the

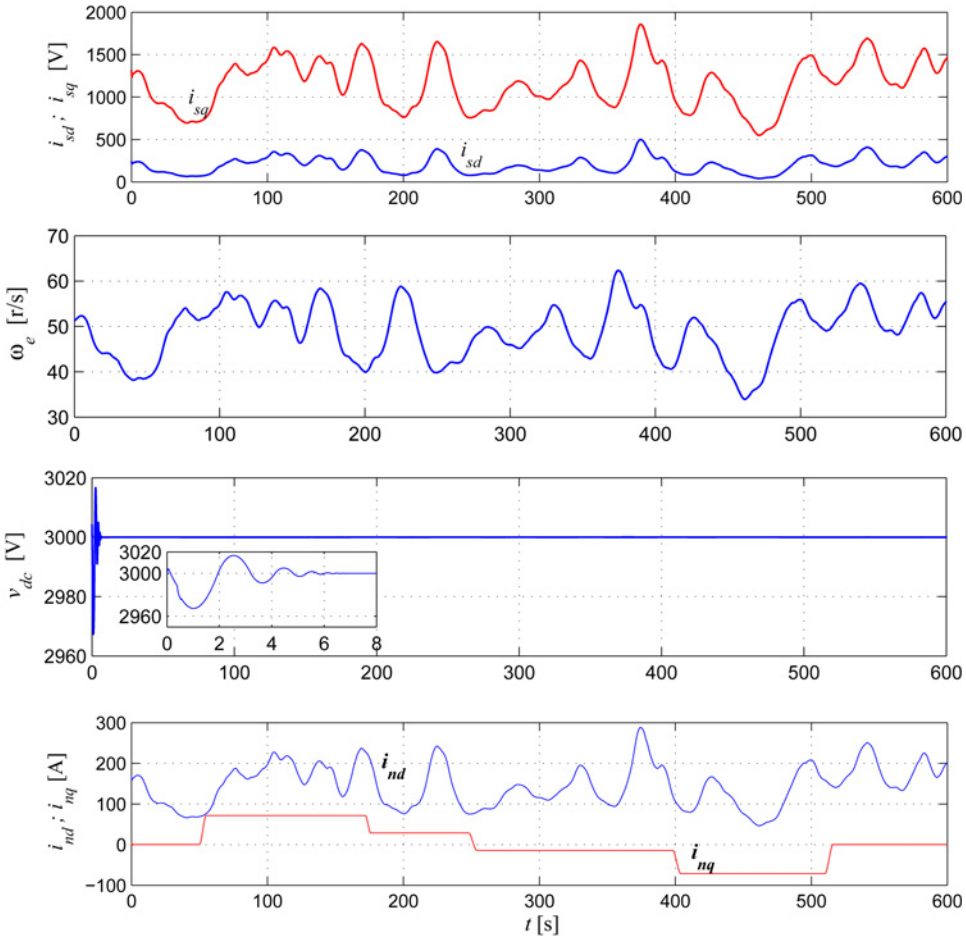

Fig. 6 *System variables i_{sd}, i_{sq}, ω_e, v_{dc}, i_{nd} and i_{nq}*

previous section, a sudden grid voltage drop triggers a switch in the control outputs. The SOSM controllers acting on s_1 and s_2 are temporarily replaced by a pair of feed-forward controllers that try to keep the currents i_{nd} and i_{nq} in similar levels than before the voltage fault. In this way the active power transferred to the grid falls but the currents are maintained near the values that they would have after the fault. Besides, during this voltage dip the inputs of the SOSM controllers are frozen (inputs forced to zero) to avoid wind-up effects. The overall result of all these actions is to dramatically reduce over speeds on the shaft, over voltages on the DC-bus and large currents on the grid side inverter, avoiding wind turbine disconnections during faults, providing at the same time a fast recovering. The results of the assumed control strategy can be appreciated from Figs. 8 to 10 where the temporal profiles of the main variables are depicted.

Fig. 8 depicts the behaviour of the control signals of the grid side inverter. As it can be seen, the input u_{nd} presents an abrupt drop produced by the active power reference fall. In the case of the input u_{nq}, at $t = 1$ s this figure shows the control switching to the feed-forward option, which try to maintain the current levels before the fault (see Fig. 9). After the voltage dip, this control signal presents a small oscillation produced by the system rearrangement (operational point change).

Fig. 9 presents the temporal variations of the grid side inverter currents. It can be appreciated the action of the feed-forward control between $t \in [1, 2]$s which try to maintain the current values existing before the fault. After it, the current values evolve to the new operational point which should be in the neighbourhood of the previous one (before the fault).

Finally, in Fig. 10 the temporal profiles of the DC-bus voltage and the mechanical shaft speed are shown. It can be appreciated in these images the good performance of the proposed control scheme. The DC-bus voltage experiment a very low overvoltage with a short oscillation after the fault. On the other hand, the mechanical shaft speed does not present significative changes and its oscillation is quickly mitigated.

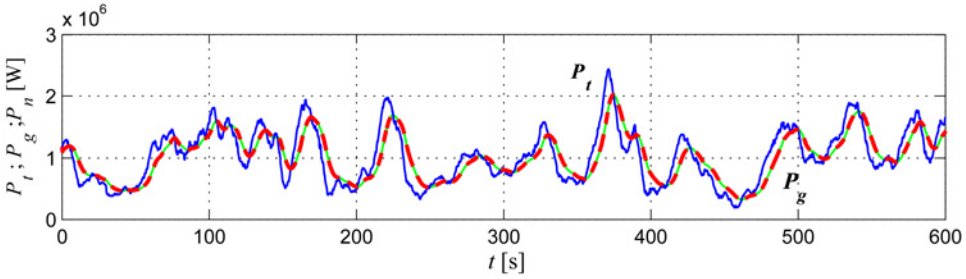

Fig. 7 *Mechanical and active electrical powers*

IET Renew. Power Gener., 2015, Vol. 9, Iss. 8, pp. 925–934

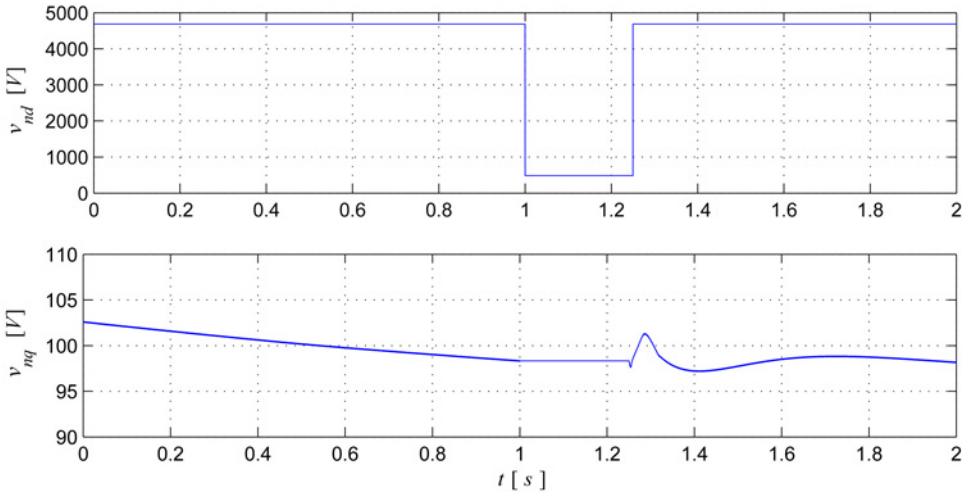

Fig. 8 *Grid side inverter control actions during 3PGF*

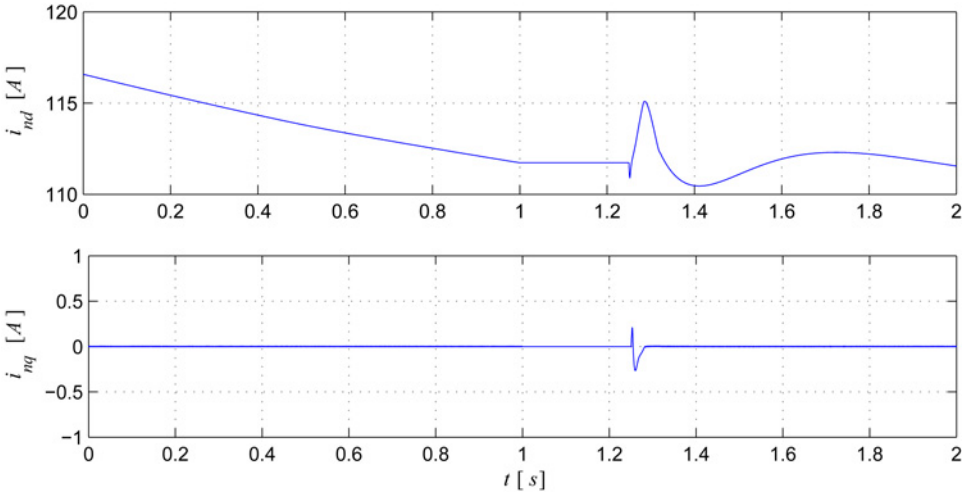

Fig. 9 I_{nd} *and* I_{nq}

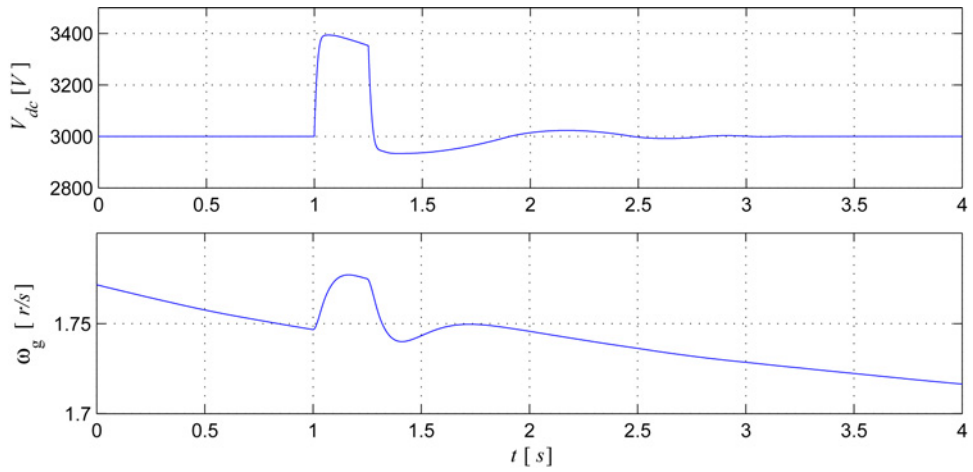

Fig. 10 V_{dc} *and* ω_g

5 Conclusions

A two-layers control scheme developed into the theoretical framework of SOSMs was presented and tested by simulations on a particular grid connected WECS. During normal operation, the first control layer involves a MIMO–SOSM controller that, acting on the grid side inverter, maximises the active power injected into the grid and regulates the reactive power according to the grid

operator directives. On the other hand, acting on the generator inverter side this controller regulates the quadrature current on the generator which indirectly maintains the DC-bus voltage level. The reference of this last control objective is obtained from an SISO–SOSM controller placed on the second layer of the proposed control scheme. This last controller adjusts an auxiliary reference that avoid errors in the DC-bus voltage level. The sliding mode variables proposed in this paper determine a control structure that allows a direct control assignment providing for an easier control design task. The control technique used to design these controllers (SOSM–STwA) allows dealing with complex non-linear systems providing simple and robust controllers that take the system to fulfil the control objectives in finite time.

6 References

1 Hansen, A.D., Cutuluis, N.A., Sorensen, P.E.: 'Impact of fault ride through requirements on fixed speed wind turbine structural loads', *Wind Energy*, 2011, **14**, pp. 1–11

2 Tsili, M., Papathanassiou, S.: 'A review of grid code technical require-ments for wind farms', *IET Renew. Power Gener.*, 2009, **3**, (3), pp. 308–332

3 Zhang, F., Leithead, W.E., Anaya-Lara, O.: 'Wind turbine control design to enhance the fault ride through capability'. Proc. IET Conf. Renewable Power Generation, Edinburgh, UK, September 2011, pp. 1–6

4 Ahuja, H., Bhuvaneswari, G., Balasubramanian, R.: 'Ride through of grid faults for PMSG based wind energy conversion systems'. Proc. Seventh IEEE Int. Conf. Industrial and Information Systems (ICIIS), Madras, India, August 2012, pp. 1–6

5 Gkavanoudis, S., Demoulias, C.: 'A new fault ride-through control method for full-converter wind turbines employing supercapacitor energy storage system'. Proc. 47th Int. Conf. Universities Power Engineering (UPEC), Edinburgh, UK, September 2012, pp. 1–6

6 Martinez, M.I., Susperregui, A., Tapia, G., Xu, L.: 'Sliding-mode control of a wind turbine-driven double-fed induction generator under non-ideal grid voltages', *IET Renew. Power Gener.*, 2013, **7**, pp. 370–379

7 Rosyadi, M., Muyeen, S.M., Takahashi, R., Tamura, J.: 'Low voltage ride through capability improvement of wind farms using variable speed permanent magnet wind generator'. Proc. Int. Conf. Electrical Machines and Systems (ICEMS), Beijing, China, August 2011, pp. 1–6

8 Semken, R.S., Polikarpova, M., Roytta, P., *et al.*: 'Direct-drive permanent magnet generators for high-power wind turbines: benefits and limiting factors', *IET Renew. Power Gener.*, 2012, **6**, pp. 1–8

9 Belloni, F., Chiumeo, R., Gandolfi, C.: 'Fault ride through strategies for permanent magnets wind generators'. Proc. Int. Symp. Power Electronics, Electrical Drives, Automation and Motion (SPEEDAM), Naples, Italy, June 2012, pp. 13–18

10 Zavvos, A., McDonald, A., Mueller, M.: 'Optimisation tools for large permanent magnet generators for direct drive wind turbines', *IET Renew. Power Gener.*, 2013, **7**, pp. 163–171

11 Ramtharan, G., Arulampalam, A., Ekanayake, J.B., Hughes, F.M., Jenkins, N.: 'Fault ride through of fully rated converter wind turbines with ac and dc transmission systems', *IET Renew. Power Gener.*, 2009, **3**, (4), pp. 426–438

12 Hansen, A.D., Michalke, G.: 'Multi-pole permanent magnet synchronous generator wind turbines grid support capability in uninterrupted operation during grid faults', *IET Renew. Power Gener.*, 2008, **3**, (3), pp. 333–348

13 Hansen, A.D., Michalke, G.: 'Modelling and control of variable-speed multi-pole permanent magnet synchronous generator wind turbine', *Wind Energy*, 2008, **11**, (5), pp. 537–554

14 Weng, Y.T., Hsu, Y.Y.: 'Sliding mode regulator for maximum power tracking and copper loss minimisation of a doubly fed induction generator', *IET Renew. Power Gener.*, 2014, pp. 297–305

15 Levant, A.: 'Sliding order and sliding accuracy in sliding mode control', *Int. J. Control*, 1993, **58**, (6), pp. 1247–1263

16 Levant, A.: 'MIMO 2-sliding control design'. Proc. European Control Conf., Cambridge, UK, September 2003, pp. 1–6

17 Benbouzid, M., Beltran, B., Amirat, Y., Yao, G., Han, J., Mangel, H.: 'High-order sliding mode control for DFIG-based wind turbine fault ride through'. Proc. 39th IEEE Conf. Industrial Electronics Society, IECON 2013, Vienna, Austria, November 2013, pp. 7670–7674

18 Shtessel, Y., Taleb, M., Plestan, F.: 'A novel adaptive-gain supertwisting sliding mode controller: methodology and application', *Automatica*, 2012, **48**, pp. 759–769

19 Susperregui, A., Martinez, M.I., Tapia, G., Vechiu, I.: 'Second-order sliding-mode controller design and tuning for grid synchronisation and power control of a wind turbine-driven doubly fed induction generator', *IET Renew. Power Gener.*, 2013, **7**, pp. 540–551

20 Rolan, A., Luna, A., Vazquez, G., Aguilar, D., Azevedo, G.: 'Modeling of a variable speed wind turbine with a permanent magnet synchronous generator'. Proc. IEEE Int. Symp. Industrial Electronics, Seoul, Korea, July 2009, pp. 734–739

21 Shtessel, Y., Plestan, F., Taleb, M.: 'Lyapunov design of adaptive supertwisting controller applied to a pneumatic actuator'. Proc. 18th IFAC World Congress, Milano-Italy, August 2011, pp. 3051–3056

22 Valenciaga, F.: 'Active and reactive power control of a brushless doubly fed reluctance machine using high order sliding modes'. Proc. Int. Conf. Electrical Machines (ICEM2008), Vilamoura, Portugal, September 2008, pp. 1–6

23 Levant, A.: 'Introduction to high-order sliding modes', in available at http://www.tau.ac.il/levant/hosm2002.pdf, 2003

24 Valenciaga, F., Evangelista, C.: '2-sliding active and reactive power control of a wind energy conversion system', *IET Control Theory Appl.*, 2009, **4**, (11), pp. 2479–2490

25 Evangelista, C., Puleston, P., Valenciaga, F., D'avila, A.: 'Variable gains super-twisting control for wind energy conversion optimization'. Proc. 11th Int. Workshop on Variable Structure Systems, Mexico City, Mexico, June 2010, pp. 50–55

26 Wu, B., Lang, Y., Zargari, N., Kouro, S.: 'Power conversion and control of wind energy systems', Hanzo, L. (Ed.): Power Conversion and Control of Wind Energy Systems (Wiley – IEEE Press, Hoboken, New Jersey, 2011)